Journal of Biomedical Optics

BiomedicalOptics.SPIEDigitalLibrary.org

# Interferometric time-stretch microscopy for ultrafast quantitative cellular and tissue imaging at 1 $\mu$m

Andy K. S. Lau
Terence T. W. Wong
Kenneth K. Y. Ho
Matthew T. H. Tang
Antony C. S. Chan
Xiaoming Wei
Edmund Y. Lam
Ho Cheung Shum
Kenneth K. Y. Wong
Kevin K. Tsia

SPIE.

# Interferometric time-stretch microscopy for ultrafast quantitative cellular and tissue imaging at 1 $\mu$m

**Andy K. S. Lau,[a] Terence T. W. Wong,[a,†] Kenneth K. Y. Ho,[b,‡] Matthew T. H. Tang,[b] Antony C. S. Chan,[a] Xiaoming Wei,[a] Edmund Y. Lam,[a] Ho Cheung Shum,[b,c] Kenneth K. Y. Wong,[a] and Kevin K. Tsia[a,*]**
[a]University of Hong Kong, Faculty of Engineering, Department of Electrical and Electronic Engineering, Pokfulam Road, Hong Kong, China
[b]University of Hong Kong, Faculty of Engineering, Department of Mechanical Engineering, Pokfulam Road, Hong Kong, China
[c]University of Hong Kong-Shenzhen Institute of Research and Innovation, Shenzhen Software Park, Shenzhen, China

**Abstract.** Quantitative phase imaging (QPI) has been proven to be a powerful tool for label-free characterization of biological specimens. However, the imaging speed, largely limited by the image sensor technology, impedes its utility in applications where high-throughput screening and efficient big-data analysis are mandated. We here demonstrate interferometric time-stretch (iTS) microscopy for delivering ultrafast quantitative phase cellular and tissue imaging at an imaging line-scan rate >20 MHz—orders-of-magnitude faster than conventional QPI. Enabling an efficient time-stretch operation in the 1-$\mu$m wavelength window, we present an iTS microscope system for practical ultrafast QPI of fixed cells and tissue sections, as well as ultrafast flowing cells (at a flow speed of up to 8 m/s). To the best of our knowledge, this is the first time that time-stretch imaging could reveal quantitative morphological information of cells and tissues with nanometer precision. As many parameters can be further extracted from the phase and can serve as the intrinsic biomarkers for disease diagnosis, iTS microscopy could find its niche in high-throughput and high-content cellular assays (e.g., imaging flow cytometry) as well as tissue refractometric imaging (e.g., whole-slide imaging for digital pathology).  [DOI: 10.1117/1.JBO.19.7.076001]

Keywords: time-stretch imaging; high-speed microfluidic; cell imaging; ultrafast frame rate; biophotonics; imaging flow cytometry; high throughput.

Paper 140059R received Jan. 31, 2014; revised manuscript received May 21, 2014; accepted for publication May 29, 2014; published online Jul. 1, 2014.

## 1 Introduction

The ability of retrieving a wealth of quantitative information from biological specimens at both the tissue and cellular levels is crucial in biomedicine for accurate disease diagnosis and prognosis, particularly in the context of high-throughput and high-content screening. Examples include the pressing need for single-cell analysis, which aims to assess cell-to-cell heterogeneity within a large population of cells ($>10^6$ cells),[1] and whole-slide imaging (WSI) which involves high-throughput histological examination for the emerging field of digital pathology.[2] The functional and structural information of the biological cells and tissues can commonly be inferred by the correlated image contrasts. While exogenous fluorescent labels are the well-acclaimed and, thus, the prevalent contrast agent used in many applications, they are not always ideal in view of the complications introduced by cytotoxicity and photobleaching. In contrast, endogenous image contrast, e.g., absorption and scattering, could sometimes serve as an effective intrinsic biomarker without the need for label or stain and the associated laborious sample preparation procedures. Among different label-free optical imaging modalities, quantitative phase imaging (QPI) has proven to be an effective approach to scavenge different useful intrinsic information about cells and tissues. By mapping the optical phase shift across the transparent cells or tissues, QPI can not only provide noninvasive high image contrast, but also quantitative evaluation of cellular information (e.g., cell volume, mass, refractive index, stiffness, membrane tension) at a nanometer scale based on the optical phase.[3] The scattering properties of the cells/tissues can also be extracted from the optical phase.[4–6] All information derived from QPI can then be used as the intrinsic biomarkers for cellular identification and for understanding the corresponding physiological information, such as the disease state of cells/tissues.[5–8] However, such high-information-content measurements of innumerable cells or large-area tissues generally demand a high-throughput imaging capability, which directly links to the image acquisition rate of QPI. Essentially, the same as all other classical optical imaging systems, the fact that QPI mostly requires image sensors for image acquisition means it falls into the common trade-off area between imaging sensitivity and speed.

A new optical imaging concept, called serial time-encoded amplified microscopy or, generally, time-stretch microscopy, has recently been developed to achieve an ultrafast imaging frame rate.[9–12] The optical amplification implemented in time-stretch microscopy enables a frame rate beyond megahertz without significantly sacrificing the detection sensitivity. Running in a line-scan mode, time-stretch microscopy has been demonstrated in ultrafast cellular unidirectional flow imaging at a speed not achievable by any conventional image sensors.[13] It can also be combined with other types of laser

*Address all correspondence to: Kevin K. Tsia, E-mail: tsia@hku.hk

†Current address: Washington University in St. Louis, Faculty of Engineering, Department of Biomedical Engineering, St. Louis, Missouri 63130

‡Current address: University of Michigan, Faculty of Engineering, Department of Mechanical Engineering, Ann Arbor, Michigan 48109

0091-3286/2014/$25.00 © 2014 SPIE

scanners, e.g., an acousto-optic deflector, to achieve general-purpose high-speed imaging.[14] Motivated by the fact that this technology is intrinsically compatible with label-free phase contrast imaging, here we demonstrate interferometric time-stretch (iTS) microscopy in the 1-$\mu$m wavelength regime for quantitative phase contrast tissue and cellular imaging at an ultrahigh imaging scan rate as high as 26 MHz, with nanometer precision. While early demonstrations of time-stretch imaging mainly operate at the telecommunications band ($\sim$1550 nm),[9,13,15] it is more desirable to explore time-stretch imaging in the shorter wavelength regime, particularly $\sim$1 $\mu$m. Apart from achieving higher diffraction-limited resolution by moving to shorter wavelengths, this 1-$\mu$m spectral window is more favorable for a wider range of biophotonic applications, especially *in vivo* imaging[16] and microfluidic imaging.[17] In contrast to our recent work on time-stretch microscopy in this wavelength window,[10] here we enable the capability of revealing quantitative phase information of the biological specimen in 1-$\mu$m time-stretch microscopy by the use of interferometry. Specifically, we present an iTS microscope system that is capable of delivering quantitative phase microscopy (QPM) of fixed cells and tissue sections, as well as ultrafast flowing cells in the 1-$\mu$m wavelength window with a line-scan rate up to 26 MHz. iTS microscopy greatly surpasses the acquisition speed of the conventional QPM without a significant loss of sensitivity. We thus anticipate that iTS microscopy could find its niche in ultrafast QPI for high-throughput cellular assays (e.g., imaging flow cytometry) as well as tissue imaging (virtual microscopy for WSI).

## 2 Experimental Setup and Principles

### 2.1 *Experimental Setup*

The general schematic of the iTS microscope setup is depicted in Fig. 1. In this paper, two different types of pulsed laser sources were chosen for different iTS microscopy demonstrations: (1) source A: a home-built fiber mode-locked laser (center wavelength = 1064 nm, bandwidth = 10 nm, repetition rate = 26.3 MHz) with preamplification by a home-made ytterbium-doped fiber amplifier (YDFA) (net optical gain = $\sim$6 dB), which is then prechirped by a 5-km single-mode fiber (SMF, Nufern 1060XP) and further amplified by a YDFA (with net optical gain of $\sim$25 dB)[18] and (2) source B: a broadband pulsed laser (bandwidth = 60 nm) generated through supercontinuum generation in a highly nonlinear fiber (431C, length = $\sim$100 m), pumped by a pulsed laser (Time-bandwidth Products Ltd., Switzerland, center wavelength = 1064 nm, repetition rate = 20 MHz). The pulsed laser beam is first split into two paths through a beam splitter (power splitting ratio = 55:45), forming a reference path and a sample path in a Michelson interferometer configuration. A one-dimensional (1-D) spectral shower is diffracted by passing the sample beam through a diffraction grating (Richardson Gratings Ltd., Rochester, New York, groove density = 1200 lines/mm, Littrow angle = 42.1 deg) and illuminates the samples. By a double-pass transmission configuration using two objective lenses (both with NA = 0.66), the spatial coordinates are mapped to the wavelength spectrum of the 1-D spectral shower. This is a process called spectral encoding.[19,20] The spectrally encoded pulsed beam from the sample arm is then interfered with its uncoded replica from the reference arm by the same beam splitter. The combined beam is then coupled into a dispersive fiber by a fiber collimator. The interfered pulses undergo optical time-stretch (also known as dispersive Fourier transform[21,22]) along the dispersive fiber through group velocity dispersion (GVD). The dispersive fiber modules used with sources A and B are different: (1) a 13-km few-mode fiber (FMF, SMF28) with a total GVD value of $\sim$0.45 ns/nm for source A and (2) a 5-km SMF (Nufern 1060XP) and a 6-km FMF (SMF28) with total GVD value of $\sim$0.35 ns/nm for source B. FMF has been found to be an effective dispersive fiber option for the time-stretch process with a selective mode excitation.[23] With these GVDs, the time-stretched interferograms can be completely resolved and the diffraction limited resolution is preserved.[12,17] The time-stretch interferograms are also amplified by an in-line YDFA, which achieves an on-off gain as high as $\sim$15 dB in order to compensate for the dispersive loss and, thus, enhance the imaging sensitivity. Afterward, a high-speed (electrical bandwidth = 8 GHz) single-pixel photo-detector with a sensitivity (NEP = $-$19 dBm) and a real-time oscilloscope (electrical bandwidth = 16.8 GHz, sampling rate = 80 GS/s) is used to digitize and acquire the temporal interferograms. To acquire a two-dimensional (2-D) image, the sample is line-scanned in the direction orthogonal to the spectral shower's main axis in the case of imaging fixed cells and tissues, or the unidirectional flow of the cells naturally provides the orthogonal image scan in the case of microfluidic flow imaging.

### 2.2 *Image Reconstruction of iTS Microscopy*

The quantitative phase image of the sample is retrieved in a way similar to conventional QPI.[24] In the case of reconstructing the iTS images, an additional step is required, i.e., transformation of the temporal interferograms into the spatial ones. Such mapping between space and time can be calibrated through the relation[25] $\delta x = \delta t \times C/\mathrm{GVD}$, where $\delta x$ and $\delta t$ correspond to the changes in space and time, respectively. $C$ is the conversion factor between the space and wavelength that is governed by the spatial dispersion law of the diffraction grating.[25] Once the mapping is known, the temporal interferograms obtained from the oscilloscope can be expressed in the following spatial form:[26]

$$I(x) = I_R + I_S(x) + 2\sqrt{I_R \times I_S(x)} \cdot \cos\{2[k(x)\Delta z + \phi(x)]\}, \quad (1)$$

where $I_R$ and $I_S(x)$ are the intensity of the reference and sample beams, respectively, $\phi(x)$ is the phase information of the specimen, which is determined by the sample morphology and refractive index, $k(x)$ is the wave vector along the x-direction, i.e., the wavelength, and $\Delta z$ is the optical path length difference between the sample and reference arms. The intensity signal, $I(x)$, is first digitally high-pass filtered to suppress the low-frequency and dc terms, i.e., $I_R$ and $I_S(x)$. Hence, the fast-oscillating cosine term, $\cos\{2[k(x)\Delta z + \phi(x)]\}$, can be isolated for phase retrieval. Hilbert transformation is then performed on the fast-oscillating cosine function, such that the phase term can be obtained by taking the arc-tangent operator of the complex analytical function in Eq. (2)

$$f(x) = I_i(x) \cdot \cos[\varphi(x)] + i \cdot I_i(x) \cdot \sin[\varphi(x)], \quad (2)$$

$$\varphi(x) = \tan^{-1}\frac{\mathrm{Im}[f(x)]}{\mathrm{Re}[f(x)]}, \quad (3)$$

where $I_i(x) = 2\sqrt{I_R \times I_S(x)}$ and $\varphi(x) = 2[k(x)\Delta z + \phi(x)]$.

Since the phase term retrieved from the tangent operation has limits between $-\pi$ and $+\pi$, a 2-D phase unwrapping algorithm,

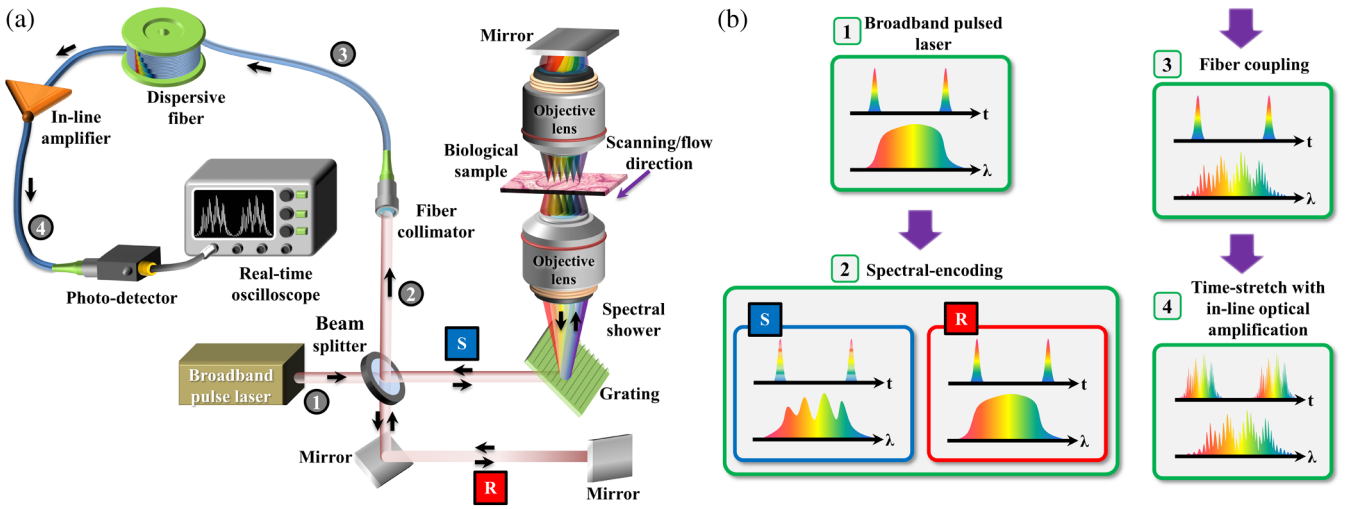


**Fig. 1** Interferometric time-stretch (iTS) microscope setup. (a) A broadband pulsed laser is used for generating a one-dimensional spectral shower after passing through a diffraction grating, which is then focused onto the sample plane by an objective lens. Built upon a Michelson interferometer configuration, the setup recombines the double-passed, spectrally encoded sample beam (S) with the reference beam (R) by the beam splitter. The interfered pulsed beams are coupled into the dispersive fiber by the fiber collimator. Time-stretch takes place in the dispersive fiber. An in-line amplifier is added in order to compensate the dispersive loss. Note that the group velocity dispersion should be large enough to provide sufficient time-stretch for preserving the diffraction-limited resolution. The time-stretched interferograms are detected by the single-pixel photodetector and a real-time oscilloscope. Phase retrieval and unwrapping are done off-line to reconstruct the quantitative phase information. (b) The corresponding temporal and spectral waveforms in different stages [steps 1 to 4 as shown in (a)]. R and S refer to the reference and the sample arms in a Michelson interferometer configuration.

Goldstein's algorithm, is applied to obtain the unwrapped true phase from the discontinuous wrapped phase. Such 2-D phase unwrapping of a $200 \times 3000$ points image can be done within 2 min by a custom-written MATLAB® code run on a personal computer.

It should be noted that the image resolution of iTS is essentially defined in the same way as the original time-stretch microscopy, as discussed in detail elsewhere.[10,25] In brief, the resolution of iTS is governed by three different limiting regimes, each of which is dominated by (1) the spectral resolution of the diffraction grating (spatial-dispersion limited), (2) the spectral resolution defined by stationary-phase approximation (SPA) in the time-stretch process (SPA-limited), or (3) the temporal resolution of the digitizer (digitizer-limited). Each of these limiting cases has an associated spatial resolution, and the final image resolution is defined as the maximum of these three values. It is desirable that the resolution should be ultimately limited by the spatial dispersion (i.e., spectral encoding process). Based on our current system configuration and following the analysis presented in Ref. 25, our current system design yields a resolution limited by spatial dispersion and is calculated to be $\sim$1.2 $\mu$m—sufficient for cellular imaging, as will be shown in a later section.

## 3 Results

### 3.1 *Basic Performance of iTS Microscopy*

To first demonstrate the quantitative imaging capability of iTS, we image an ISO 12233 resolution chart, which is fabricated by depositing a thin layer of photo-resist (MicroChem Corp., Newton, Massachusetts, Shipley 1805, refractive index $\sim$1.52 at 1064 nm, thickness of $\sim$400 nm) on a glass slide, by the iTS microscope based on source B. By taking an average of 20 single-shot line-scans, we can achieve an effective line-scan rate as high as 1 MHz. The 2-D interferogram is obtained by scanning the resolution chart in the orthogonal direction with a step size of 0.5 $\mu$m. Figures 2(a) and 2(b) show the bright-field image taken by the conventional optical microscope and the iTS microscopic image of the same area of the resolution chart. iTS can not only show a similar image quality at the ultrafast line-scan rate of 1 MHz, but can also reveal the quantitative height profile. We validate the performance of such ultrafast noncontact profilometry by comparing the height profile measured by iTS with that measured by a profilometer (Dektak XT, Bruker Corp., Germany), as shown in Fig. 2(c).

We also image the oil-in-water emulsion droplets by iTS as another proof-of-principle experiment by using source A [Fig. 2(d)]. The droplets are generated through the flow focusing scheme in a home-made microfluidic channel and are then transferred to a glass slide covered by the coverslip. We note that high-speed quantitative characterization of droplet emulsion formation is crucial for high-throughput monitoring and screening during drug encapsulation.[27,28] With the known refractive indices of water (1.327) and silicone oil (1.40), the iTS microscope, running at a 1 MHz line-scan rate, is able to retrieve the quantitative morphology of the emulsion. The flat-top profile of the emulsion (with a thickness of $\sim$2 $\mu$m) is attributed to the droplet being compressed by the coverslip.

To verify the stability and accuracy of the phase acquired by the current iTS microscope, we measure the phase of the 1-D iTS line-scan for a total time of 95 s at a line-scan rate of 26 MHz. The phase stability/variation is defined as the standard deviation of phase within a diffraction-limited focused spot and is found to be 0.01 rad [Fig. 2(e)]. This is comparable to the phase stability of the conventional QPI system, but is achieved

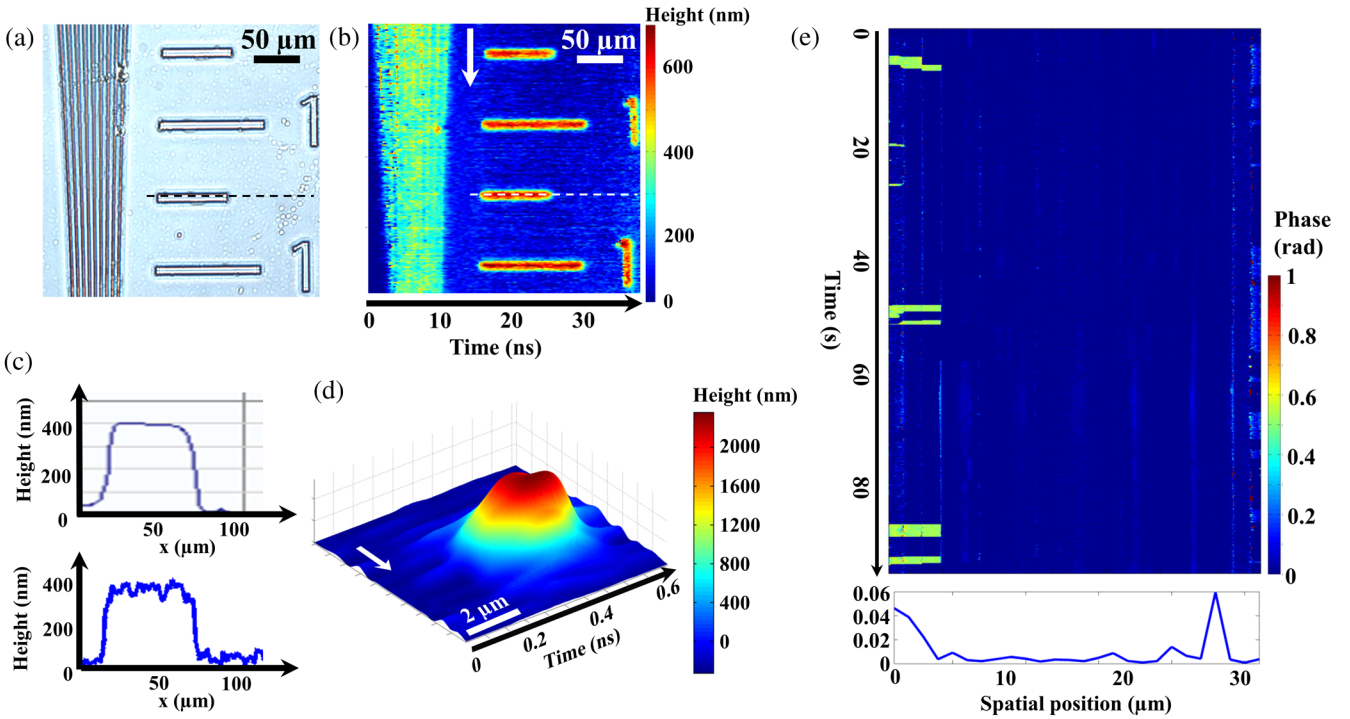


**Fig. 2** Basic performance of iTS microscopy. (a) ISO 12233 resolution chart captured by bright-field light microscope. (b) Same region of resolution chart captured by iTS microscope at 1 MHz line-scan rate. The color bar shows the corresponding height. (c) Height profile along dashed line in (a) to (b) measured by profilometer (top) and iTS microscopy (bottom). (d) Tomographic image of an oil-in-water emulsion obtained by iTS microscopy at 1 MHz line-scan rate. The height profile is evaluated by the known refractive indices of water (1.33) and silicone oil (~1.40). Inset shows the corresponding three-dimensional tomography of the emulsion droplet. (e) 1000 sampled line-scans of quantitative phase captured by the iTS microscope within 95 s. The bottom inset shows the average temporal phase stability along the spectral shower direction. The overall phase stability along the spectral shower direction is 0.01 rad, which is comparable to conventional quantitative phase imaging. Arrows indicate scanning direction.

at an orders-of-magnitude faster imaging speed.[24] Further improvement in phase stability can be obtained with a pulse laser source with better temporal power stability.

### 3.2 *Quantitative Cellular and Tissue Imaging by iTS Microscopy*

We also demonstrate iTS imaging (using source B) of both the cell culture samples and tissue section samples mounted on the glass slides. By scanning the unstained nasopharyngeal epithelial cells in the direction orthogonal to the spectral shower with a step size of 0.5 $\mu$m, a 2-D iTS image can be acquired. The morphology of the epithelial cells [Fig. 3(a)] can be revealed by iTS microscopy when compared with the classical phase contrast images on the same region of interest [Fig. 3(b)]. More importantly, iTS imaging can also retrieve the quantitative phase profile of the cells at an ultrahigh line-scan rate of 1 MHz. We note that the extracted phase information can be used for further quantitative analysis of the characteristics of the individual cells, e.g., sphericity, cell dry mass, etc.[3] Combined with a continuously running automated scanner similar to the ones adopted in WSI scanners but operated at a significantly higher speed, e.g., >1 m/s, an iTS microscope could be an attractive tool for boosting the throughput of WSI of biological specimens, opening up new opportunities for big-data analysis in biomedical diagnostics as well as basic life science studies. As an example, the scanning speed of the commercially available WSI scanners is severely impeded by the speed limitation of the current camera technology. Compromising the camera speed, today's scanners require >1 min to scan a typical area 1.5 × 1.5 cm at 20× magnification.[2] Furthermore, in some applications such as digital pathology, that rescanning is often required. As a result, a WSI system with ultrafast iTS microscopy could be of great value for realizing truly high-throughput quantitative screening.

We further demonstrate this potential by performing large-area iTS imaging of a tissue section on a slide (using source B). By scanning the tissue in the orthogonal direction with a step size of 1 $\mu$m at a 1 MHz line-scan rate, a 2-D iTS image of the tissue section is acquired. A large-area iTS image of the tissue section (~500 $\mu$m × 1000 $\mu$m is then formed by stitching 10 iTS subimages. The refractive index map of the spleen tissue quantified by iTS microscopy is shown in Fig. 3(c), which is morphologically consistent with the H&E-stained tissue captured by a bright-field optical microscope in the same area [Fig. 3(d)]. The heterogeneous refractive index distribution of spleen tissue is evaluated by taking the known refractive index of the surrounding phosphate bovine solution, which is 1.331 at 1 $\mu$m, and the known thickness of the sectioned tissue, which is 5 $\mu$m. Once again, the iTS microscope is able to reveal quantitative intrinsic information (refractive index in this case) of the tissue with cellular resolution and at a 1 MHz line-scan

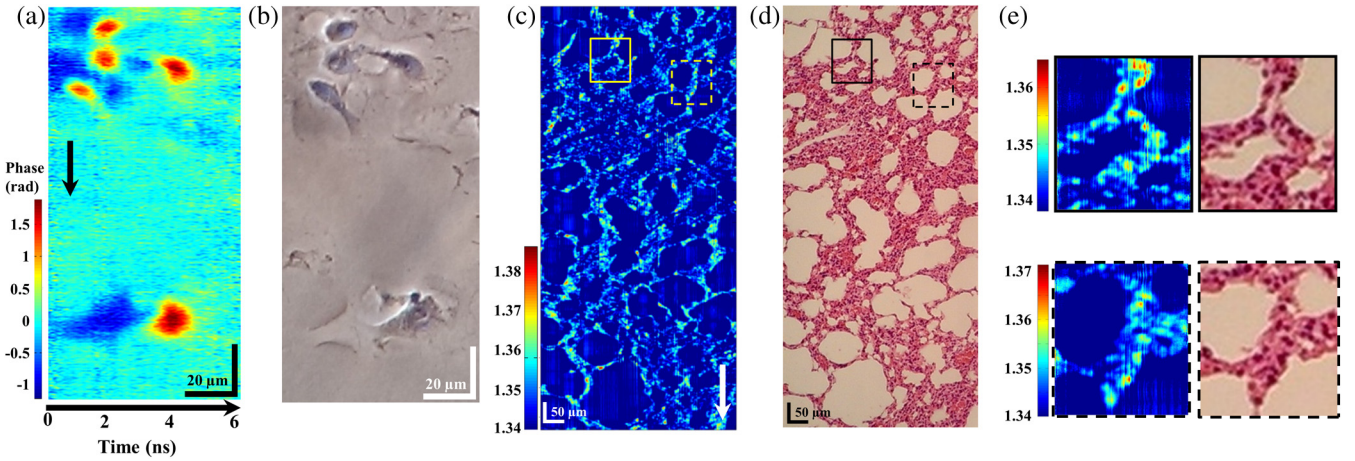


**Fig. 3** iTS microscopy of fixed cells and tissues on slides. (a) Nasopharyngeal epithelial cells captured by iTS microscopy at 1 MHz line-scan rate. (b) Same region of cells captured by conventional phase contrast microscopy. The color bar represents the quantitative phase values in radian. (c) Spleen tissue image captured by iTS microscopy at 1 MHz line-scan rate by stitching 10 iTS subimages. It is in good agreement morphologically with the bright-field image of the tissue with H&E stain. (e) Zoom-in views of the highlighted areas shown in (c) and (d). Color bars in (d) and (e) show the refractive index values. Arrows indicate scanning direction.

rate. Similar to the conventional QPI modalities, the quantitative phase image acquired by iTS microscopy can obtain not only the spatial distribution of the tissue refractive index, but also the scattering mean free path as well as the anisotropy factor.[7] As these parameters can be regarded as the effective intrinsic biomarkers for new types of label-free disease diagnosis,[8] iTS imaging has the unique advantage of making high-throughput WSI-based quantitative tissue histopathology possible.

### 3.3 *iTS Microscopy for Quantitative Cellular Imaging in Ultrafast Microfluidic Flow*

Finally, we demonstrate iTS imaging of ultrafast flowing cells in the microfluidic platform. Two types of unstained and immortalized cell lines are used: human cervical cancer cells (HeLa) [Figs. 4(a) to 4(e)] and normal hepatocyte cells (MIHA) [Figs. 4(f) to 4(j)], flowing at the ultrahigh speed of 8 and

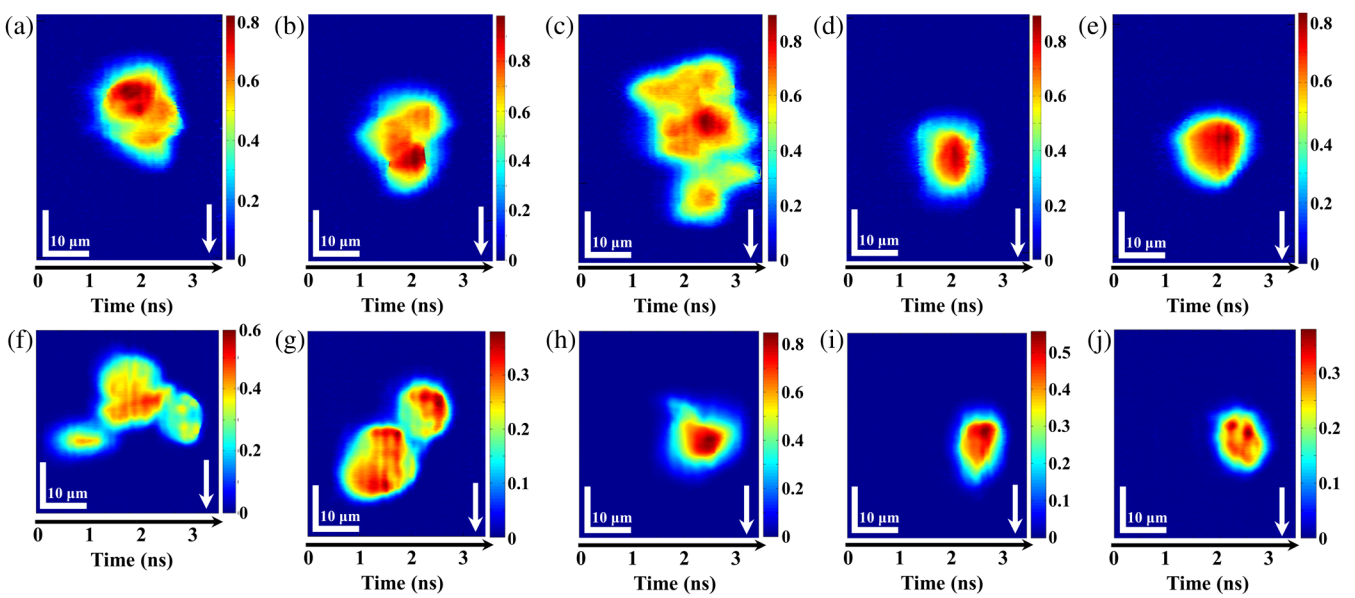


**Fig. 4** Imaging of mammalian cells by iTS microscopy in ultrafast flow. (a) to (e) iTS microscopic images of stain-free HeLa cells flowing at a speed of 8 m/s. (a) to (c) Clusters of HeLa cells can be easily distinguished under iTS microscopy with subcellular resolution (~1.2 $\mu$m. (d) and (e) Single HeLa cells flowing at ultrahigh speed. (f) to (j) iTS microscopic images of stain-free MIHA cells flowing at a speed of 0.4 m/s. (f) and (g) Clusters of MIHA cells can be easily distinguished under iTS microscopy with subcellular resolution. (h) to (j) Single MIHA cells flowing at 0.4 m/s. All color bars represent the phase in radian. Arrows indicate flow direction.

0.4 m/s in the microfluidic channel, respectively. Such flow speed range corresponds to an imaging throughput as high as ~80,000 cells/s. The ultrafast fluidic flow is accomplished by the inertial flow focusing scheme, which helps align the flowing cells at the center region of the microfluidic channel (see Appendix for detailed fabrication procedures).[29] Enabling the ultrafast line-scan rate of 26 MHz (determined by the repetition rate of source A) as well as the ultrashort exposure time of 30 ps (determined by the time-bandwidth product of each spectrally resolvable subpulse of the spectral shower[9,10]), respectively, the QPI of the fast flowing cells can be captured without image blur by iTS microscopy. This is clearly evident from the fact that the individual cells in an aggregate in such high-speed flow can be identified [see Figs. 4(a) to 4(c) and 4(f) to 4(h)]. More importantly, this is the first time, to the best of our knowledge, that heterogeneity of the subcellular morphology can also be resolved and quantified by iTS microscopy. In this ultrahigh-speed flow imaging scenario, the average phase fluctuation across 2620 line-scans was measured to be 0.00271 rad, which is practical for quantitative cellular analysis as demonstrated by the conventional QPI modalities. Operating in the cellular flow imaging scenario, iTS microscopy is a unique tool for bringing label-free quantitative phase imaging into the flow cytometry platform with an imaging throughput not achievable by any existing QPI techniques. As a result, iTS microscropy, combined with the state-of-the-art flow cytometer, could be of great value for quantitative single-cell analysis with high throughput as well as high content.

## 4 Conclusions

We have developed a new ultrafast quantitative phase imaging modality, iTS microscopy, which offers an imaging speed orders-of-magnitude faster than any existing QPI. In contrast to the prior work on time-stretch imaging, our present iTS system, operated in the 1-$\mu$m wavelength window, is able to provide cellular resolution and is more favorable for a wider range of bioimaging applications. Its distinctive feature of ultrahigh-speed QPI aligns well with the drive toward high-throughput and high-content screening in biomedical diagnostics as well as fundamental life science research. Specifically, we demonstrated iTS imaging of both cells and tissues fixed on slides with an imaging line-scan rate of 1 MHz, revealing quantitative phase information and the derived intrinsic cellular parameters, such as refractive index. Combined with a highly automated scanning system, iTS imaging could find a niche in boosting the throughput of the WSI of biological specimens and, thus, create new opportunities for big-data diagnosis. We also demonstrated ultrahigh-speed and high-resolution microfluidic cellular flow QPI up to 8 m/s. This corresponds to an imaging throughput as high as 80,000 cells/s, which is not attainable with any current imaging flow cytometers. As a number of useful parameters can be further scavenged from the retrieved phase image of the individual cells, we anticipate that iTS microscopy, when integrated with conventional flow cytometers, is a formidable platform for realizing label-free high-content single-cell analysis. We note that real-time iTS image reconstructions and the subsequent automated quantitative analysis require high-performance computing processors, e.g., a field-programmable gate array or graphical processing unit, in order to continuously process enormous amounts of digital data. Tailored designs in both hardware (analog-to-digital convertor and processors) and software (novel signal process algorithms) are necessary for different targeted applications based on the iTS imaging technique.

## Appendix

### A1 Methods

#### A1.1 *Microfluidic Channel Design and Fabrication*

In order to achieve the ultrahigh microfluidic flow speed as high as 8 m/s, a tailor-designed and fabricated polydimethylsiloxane-based microfluidic channel platform is used for a stable and robust quantitative phase cellular flow imaging experiment. In the design, the balance between the viscous drag force and the inertial lift force is crucial for manipulating the position of the individual cells and for focusing them, even while flowing in an ultrafast manner inside the channel. Detailed fabrication steps can be found in Ref. 17. The microfluidic platform configuration can be divided into two parts: a focusing section followed by an imaging section. In the focusing section, multiple pairs (16 turns in total) of connected curved channels with two radii of curvature, 400 and 1000 $\mu$m, respectively, are used to achieve the microfluidic focusing of individual cells. The width (150 $\mu$m) and height (50 $\mu$m) of the channel were chosen such that the channel is suitable for focusing cells with a size ranging from ~5 to 30 $\mu$m. In the imaging section where the spectral shower is illuminated onto the channel, the channel width is narrowed to 45 $\mu$m to further boost the flow speed up to ~10 m/s. Based on the Reynolds number of our current microfluidic channel design (600), which is far below the limit of 2000 (beyond which the turbulence flow occurs), this indicates that laminar flow condition is still satisfied under such an ultrafast flow.[29] To accommodate the short working distance of the high-NA objective lens used in the current system, the thicknesses of the top and bottom channel walls have been thinned to <1 mm.

#### A1.2 *Preparation of Mammalian Cell Lines—MIHA and HeLa Cells*

The HeLa cells and MIHA cells were cultured on 100-mm cell culture dish (Corning) in Dulbecco's modified eagle medium (high glucose)-HG supplemented with 10% fetal bovine serum, 100 $\mu$g/ml streptomycin, and 100 U/ml penicillin. To culture MIHA cells, sodium pyruvate was added to the culture media. All cells were cultured and grown in a humidified incubator at 37 C and 5% $CO_2$. After reaching confluence, cells in a cell culture dish were trypsinized to be suspended in an aqueous environment. Trypsin was removed by centrifuging the cell sample at 250 g for 5 min. Resuspending and fixing the cells, glutaraldehyde was added and then removed by centrifuging the cell sample by 250 g for 5 min. 1× phosphate buffered saline was added to resuspend the cells; the mixture is then loaded to the microfluidic channel for interferometric time-stretch cellular flow imaging experiments.

### *Acknowledgments*

We thank Hilary K. Y. Mak for preparing the MIHA and HeLa cell lines for us. This work was partially supported by grant from the Research Grants Council of the Hong Kong Special Administrative Region, China (Project No. HKU 7172/12E,

HKU 717510E, HKU 717911E, HKU 720112E) and University Development Fund of HKU.

## References


1. D. Anselmetti, *Single Cell Analysis: Technologies and Applications*, 1st ed., Wiley-VCH, Weinheim, Germany (2009).
2. F. Ghaznavi et al., "Digital imaging in pathology: whole-slide imaging and beyond," *Annu. Rev. Pathol. Mech.* **8**, 331–359 (2013).
3. P. Girshovitz and N. T. Shaked, "Generalized cell morphological parameters based on interferometric phase microscopy and their application to cell life cycle characterization," *Biomed. Opt. Express* **3**(8), 1757–1773 (2012).
4. Z. Wang, H. Ding, and G. Popescu, "Scattering-phase theorem," *Opt. Lett.* **36**(7), 1215–1217 (2011).
5. H. Ding et al., "Measuring the scattering parameters of tissues from quantitative phase imaging of thin slices," *Opt. Lett.* **36**(12), 2281–2283 (2011).
6. Y. K. Park et al., "Static and dynamic light scattering of healthy and malaria-parasite invaded red blood," *J. Biomed. Opt.* **15**(2), 020506 (2010).
7. N. Lue et al., "Tissue refractometry using Hilbert phase microscopy," *Opt. Lett.* **32**(24), 3522–3524 (2007).
8. Z. Wang et al., "Tissue refractive index as marker of disease," *J. Biomed. Opt.* **16**(11), 116017 (2011).
9. K. Goda, K. K. Tsia, and B. Jalali, "Serial time-encoded amplified imaging for real-time observation of fast dynamic phenomena," *Nature* **458**, 1145–1149 (2009).
10. T. T. W. Wong et al., "Optical time-stretch confocal microscopy at 1 μm," *Opt. Lett.* **37**(16), 3330–3332 (2012).
11. F. Xing et al., "Simple approach for fast real-time line-scan microscopic imaging," *Appl. Opt.* **52**(28), 7049–7053 (2013).
12. H. Chen et al., "Multiwavelength time-stretch imaging system," *Opt. Lett.* **39**(7), 2202–2205 (2014).
13. K. Goda et al., "High-throughput single-microparticle imaging flow analyzer," *Proc. Natl. Acad. Sci.* **109**, 11630–11635 (2012).
14. K. Goda et al., "Hybrid dispersion laser scanner," *Sci. Rep.* **2**, 445 (2012).
15. A. Mahjoubfar et al., "Label-free high-throughput cell screening in flow," *Biomed. Opt. Express* **4**(9), 1618–1625 (2013).
16. T. Vo-Din, Ed., *Biomedical Photonics Handbook*, CRC Press, Boca Raton, Florida, United States (2003).
17. T. T. W. Wong et al., "Asymmetric-detection time-stretch optical microscopy (ATOM) for ultrafast high-contrast cellular imaging in flow," *Sci. Rep.* **4**, 3656 (2014).
18. X. Wei et al., "Coherent laser source for high frame-rate optical time-stretch microscopy at 1.0 micron," *IEEE J. Sel. Topics Quantum Electron.* **20**, 1100306 (2014).
19. G. J. Tearney, R. H. Webb, and B. E. Bouma, "Spectrally encoded confocal microscopy," *Opt. Lett.* **23**(15), 1152–1154 (1998).
20. S. C. Schlachter et al., "Spectrally encoded confocal microscopy of esophageal tissues at 100 kHz line rate," *Biomed. Opt. Express* **4**(9), 1636–1645 (2013).
21. K. Goda and B. Jalali, "Dispersive Fourier transformation for fast continuous single-shot measurements," *Nat. Photonics* **7**, 102–112 (2013).
22. K. Goda et al., "Theory of amplified dispersive Fourier transformation," *Phys. Rev. A* **80**, 043821 (2009).
23. Y. Qiu et al., "Exploiting few mode-fibers for optical time-stretch confocal microscopy in the short near-infrared window," *Opt. Express* **20**(22), 24115–24123 (2012).
24. G. Popescu, *Quantitative Phase Imaging of Cells and Tissues*, McGraw Hill, New York, United States (2011).
25. K. K. Tsia et al., "Performance of serial time-encoded amplified microscope," *Opt. Express* **18**(10), 10016–10028 (2010).
26. M. Gronle et al., "Laterally chromatically dispersed, spectrally encoded interferometer," *Appl. Opt.* **50**(23), 4574–4580 (2011).
27. P. S. Dittrich and A. Manz, "Lab-on-a-chip: microfluidics in drug discovery," *Nat. Rev. Drug Discov.* **5**(3), 210–218 (2006).
28. P. Neuzil et al., "Revisiting lab-on-a-chip technology for drug discovery," *Nat. Rev. Drug Discov.* **11**(8), 620–632 (2012).
29. D. Di Carlo et al., "Continuous inertial focusing ordering, and separation of particles in microchannels," *Proc. Natl. Acad. Sci.* **104**, 18892 (2007).


**Andy K. S. Lau** received his BEng degree (first class honor) in medical engineering from the University of Hong Kong in 2010. He is currently working toward his PhD degree at the Department of Electrical and Electronic Engineering, University of Hong Kong. His research interests include ultrahigh-speed imaging flow cytometry through time-stretch microscopy (frame rate >10 MHz) and quantitative time-stretch microscopy for acquiring real morphology of biological samples under an ultrahigh-speed flow.

Biographies for other authors are not available.